Journal of Thermal Analysis and Calorimetry (2018) 132:317–325
https://doi.org/10.1007/s10973-017-6939-3

Investigation of the thermoelectrical properties of the $Sn_{91.2-x}$–$Zn_{8.8}$–Ag_x alloys

M. Şahin[1] · E. Çadırlı[2] · Ü. Bayram[3] · P. Ata Esener[4]

Received: 9 May 2017 / Accepted: 17 December 2017 / Published online: 28 December 2017
© Akadémiai Kiadó, Budapest, Hungary 2017

Abstract

$Sn_{91.2-x}$–$Zn_{8.8}$–Ag_x alloys ($x = 0.15$–10.0 wt%) were directionally solidified upwards at a constant G (4.16 K mm^{-1}) and V (41.5 μm s^{-1}) in a Bridgman-type directional solidification furnace. The electrical resistivity (ρ) measurements of the alloys depending on the temperature were performed using the standard four-point probe method, and the temperature coefficients of the resistivities (α) were calculated. Composition analyses of the alloys were carried out using energy-dispersive X-ray spectroscopy. The enthalpy (ΔH) and the specific heat (ΔC_p) values of the alloys were determined by differential scanning calorimetry analysis. The thermal conductivity (K) values were obtained from the Wiedemann–Franz equation. According to the experimental results, electrical resistivities increased up to 3.0 mass% Ag and decreased with further increase in Ag content. Enthalpy and specific heat values decreased with the increasing content of Ag. The results were compared with the previous works for Sn–Zn–Ag alloys.

Keywords Directional solidification · Electrical resistivity · Thermal conductivity · Enthalpy · Specific heat

Introduction

The liquid–solid phase transformation (solidification) is very important phase transformation because all metals must undergo this transformation before becoming useful materials [1]. Solidification is of such importance simply because one of its major practical applications, namely casting, is a very economic method of forming a component if the melting point of the metal is not too high [2]. One of the most important solidification methods used for material processing is the directional solidification [3]. The mechanical properties of the alloys can be improved with the directional solidification method [4–7].

In the electronics industry, solders are used as interconnect materials between electronic components and printed circuit boards. As the joining material, solders provide the necessary electrical, mechanical and thermal continuity in electronics assemblies [8–11]. Therefore, the performance and quality of the solder are crucial to ensure the proper functioning of the electronics assembly.

Unlike lead-based alloys, tin-based alloys are not harmful to health. Since welding with these alloys needs low temperature, is cost-effective and is easy to use, it is a perfect alternative to hard welding. The addition of Ag into Sn–Zn eutectic alloy is effective for improvement in the oxidation resistance [12]. The solderability of Sn–9Zn solder is significantly improved when the quantity of Ag added in the solder is 0.3 mass% [13]. The $AgZn_3$ and Ag_5Zn_8 intermetallics occur during the reflow process

✉ M. Şahin
msahin@nigde.edu.tr

E. Çadırlı
ecadirli@gmail.com

Ü. Bayram
umitbayram14@gmail.com

P. Ata Esener
pinarata_88@hotmail.com

1 Department of Electronics and Automation, Technical Vocational School of Sciences, Niğde Ömer Halisdemir University, Niğde, Turkey

2 Department of Physics, Faculty of Arts and Sciences, Niğde Ömer Halisdemir University, Niğde, Turkey

3 Department of Physics, Faculty of Science, Erciyes University, Kayseri, Turkey

4 Department of Metallurgical and Materials Engineering, Faculty of Engineering and Architecture, Nevşehir Hacı Bektaş Veli University, Nevşehir, Turkey

when Sn–Zn–Ag alloys are applied for practical uses [14]. When the Ag content is higher than 1.5 mass%, the specimens possess high damping capacity and Ag_5Zn_8 and $AgZn_3$ intermetallics increase vibration fracture resistance [15]. Nevertheless, small amount of Ag resulted in a reduction in the electrical conductivity of the Sn–Zn–Ag alloy [16]. Also, the addition of Ag into the Sn–Zn eutectic alloy improves the mechanical properties of the alloy up to a certain amount [13, 17–19].

Thus, the aim of the present work is to investigate the influence of Ag additions on the electrical and thermal properties of the directionally solidified Sn–8.8Zn eutectic solder alloy.

Experimental

Directional solidification

The directional solidification of the alloys produced by using vacuum melting furnace and casting furnace was performed in a Bridgman-type directional solidification furnace. For the directional solidification, the sample was first placed in the sample holder. The sample holder was then placed into the hot region of the furnace. After the furnace reached the desired temperature (773 K) and thermally stabilized for about 20 min, the sample was withdrawn from the hot region to the cold region of the furnace by means of constant speeded (41.5 μm s^{-1}) synchronous motor. After 14–15 cm steady-state growth, the samples were quenched by rapidly pulling it down into the water reservoir. The quenched samples were removed from the graphite, crucible and samples having a length (d) of 20–30 mm and a thickness (t) of 1 mm were cut from the directionally solidified part of the alloy for electrical resistivity measurements. Details of the furnaces equipments, alloy preparation and directional solidification are given in [20].

Measurement of electrical resistivity

The four-point probe method is the most widely used technique for electrical profile measurement of materials. The method has proved to be a convenient tool for the resistivity measurement. A four-point probe measurement is performed by making four electrical contacts to a sample surface. Two of the probes are used to measure source current and the other two probes are used to measure voltage. Using four probes eliminates measurement errors due to the probe resistance, the spreading resistance under each probe and the contact resistance between each metal probe and material [21]. The measured four-point resistance does not contain contributions from the contact resistance between the sample and the electrodes. The electrical resistivity, ρ, is determined by loading a direct current, I, through the outer pair of probes and measuring the voltage drop, V, between the inner pair of probes which are positioned at a distance of $s = 1$ mm. A total of three samples were tested for each solder alloy with 5 readings for each sample. In this study, the correction factor to be used in calculating the resistivity was determined by referring to the geometric factors in four-point resistivity measurement provided by Topsoe [22]. The "Probe Array Parallel to Edge, Thick Sample" geometric factor was chosen as it provides the closest approximation to our sample geometry. Fundamentally, the electrical resistivity is expressed as

$$\rho = G\frac{V}{I} \quad (1)$$

where G is the geometric resistivity correction factor. There is a functional relation between sample geometry and voltage (V) and current (I) that influences the electrical resistivity. In the calculation of G, which varies with sample and contact geometries, when sample dimensions $t/s \geq 1$ and $d/s < 40$ (see below) are considered, the following relation can be used [22, 23].

$$G = 2\pi s\, F_1(t/s)\, F_2(d/s) \quad (2)$$

where t and d are thickness and length of the sample, respectively, s is the distance between consecutive probes, F_1 and F_2 are additional correction factors. Consequently, G is calculated to be 0.364 cm.

The measuring unit was interfaced with a PC for the online data acquisition and processing. A Keithley 2400 source meter was used to provide constant current of 1 A, and the potential drop was detected by a Keithley 2700 multimeter. Platinum wires with a diameter of 0.5 mm were employed as current and potential electrodes. As shown in Fig. 1, outer probes are used to measure source current and the inner probes are used to measure voltage.

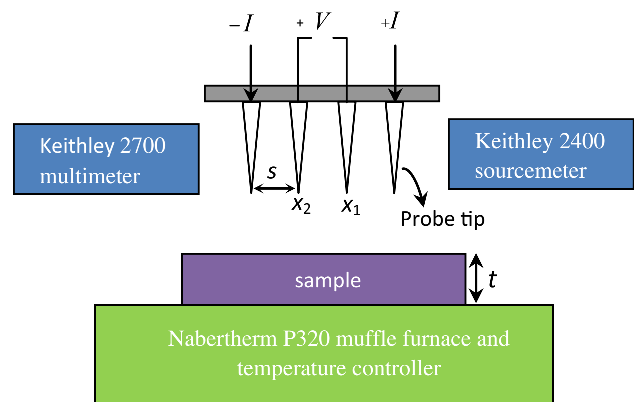

Fig. 1 Schematic diagram of the four-point probe method

The temperature of the sample in the Nabertherm P320 muffle furnace was controlled with temperature controller, and the temperature of the sample was measured with a standard *K*-type thermocouple.

The electrical resistivity strongly depends on temperature. In metals, electrical resistivity increases with increasing temperature. The dependence of electrical resistivity on the temperature is often expressed as a slope in the electrical resistivity versus temperature graph and can be given as

$$\alpha_{\mathrm{TCR}} = \frac{\rho_{\mathrm{S}} - \rho_0}{\rho_0 (T - T_0)} = \frac{1}{\rho_0}\frac{\Delta\rho}{\Delta T} \tag{3}$$

where ρ_S is the electrical resistivity at the temperature T, ρ_0 is the electrical resistivity at the room temperature and α_{TCR} is the temperature coefficient of resistivity. The error in the electrical resistivity measurements is calculated about 5%.

Calculation of thermal conductivity

Heat in solids is conducted by various carriers: electrons, lattice waves or phonons, magnetic excitations and, in some cases, electromagnetic radiation. The total thermal conductivity is additively composed of contributions from each type of carrier. The principal carriers of heat in metals are electron and lattice waves, leading to an overall thermal conductivity

$$K = K_{\mathrm{e}} + K_{\mathrm{g}} \tag{4}$$

where K_e is the electronic component and K_g is the lattice component. Generally K_g of metals, alloys and semimetals is comparable to the lattice thermal conductivity of insulators of corresponding elastic properties, except at low temperature where phonon electron interaction reduces K_g in metals. The relative importance of K_e and K_g thus depends on the magnitude of K_g. The electronic component often parallels the electrical conductivity, and the electrical conductivity is highest in pure metals, reduced in the case of alloys and even lower in semimetals and semiconductors. Electrical conductivity is a measure of a material's ability to conduct an electric current and is one of the primary physical properties of materials such as thermal conductivity, specific heat and thermal expansion. The relationship between the thermal conductivity and the electrical conductivity of metals is established by the Wiedemann–Franz equation [24] which is based on the fact that heat and electrical transport both involve the free electrons in the metal as

$$\frac{K_{\mathrm{e}}}{\sigma} = LT \tag{5}$$

where L is the constant of proportionality, which is called the Lorenz number. The value of L is 2.45×10^{-8} W Ω K^{-2} [25]. The variation of thermal conductivity (K) with temperature was determined from the Wiedemann–Franz equation by using the measured values of electrical resistivity (ρ).

Measurement of enthalpy and specific heat

At constant pressure the specific heat is expressed as

$$C_{\mathrm{p}} = \left(\frac{\partial H}{\partial T}\right)_{\mathrm{P}} \tag{6}$$

Therefore, variation of enthalpy (H) with temperature (T) can be obtained from knowledge of the variation of specific heat with temperature. Enthalpy can be measured relative to any reference level which is usually done by defining $H = 0$ at 298 K. Integration of Eq. (6) gives

$$H = \int_{298}^{T} C_{\mathrm{P}} \mathrm{d}T \tag{7}$$

At the melting temperature, the heat supplied to system will not rise its temperature but will be used supplying the enthalpy of fusion that is required to convert solid to liquid. For a transformation from to liquid state, enthalpy of fusion can be expressed as

$$\Delta H \approx \Delta C_{\mathrm{P}} T_{\mathrm{M}} \tag{8}$$

where T_M is the melting temperature and ΔC_p is the change in specific heat.

The differential scanning calorimetry (DSC) (PerkinElmer Diamond model) thermal analysis was performed with a heating rate of 10 K min^{-1} and under a constant stream of nitrogen at atmospheric pressure. The ΔH was calculated by dividing the area under the peak to the sample mass and, the ΔC_p was determined by dividing the enthalpy of fusion to the melting temperature.

Results and discussion

Composition analysis of phases

SEM–EDX analyses were performed in a Zeiss DSM 962 scanning electron microscope coupled with an Oxford Instruments INCAx sight spectrometer equipped with a Si (Li) detector (133 eV at 5.9 keV) with an ultra-thin window for the detection of low atomic number elements. Backscattered electron (BSE) imaging mode was preferred due to the high atomic number contrast. Analytical conditions comprise a working distance of 25 mm, an

accelerating voltage of 20 kV, a filament current of 3 A and an emission current of 70 μA. ZAF correction factors were applied for semi-quantifications.

Energy-dispersive X-ray analysis of the phases containing Ag in the Sn–8.8Zn–3.0Ag alloy is given in Fig. 2. From this energy-dispersive X-ray spectroscopy (EDX) analysis results, it was found that Zn has a composition of 74.58 (at.%) and Ag has a composition of 25.42 (at.%) alloy. From these EDX results and the previous studies [18, 26], this black phase shown in Fig. 2 is the $AgZn_3$ intermetallic phase. Also, the composition analyses of the intermetallic phases in the studied Sn–Zn–Ag alloys are given in Table 1, and the SEM images of the microstructures are given in Fig. 3.

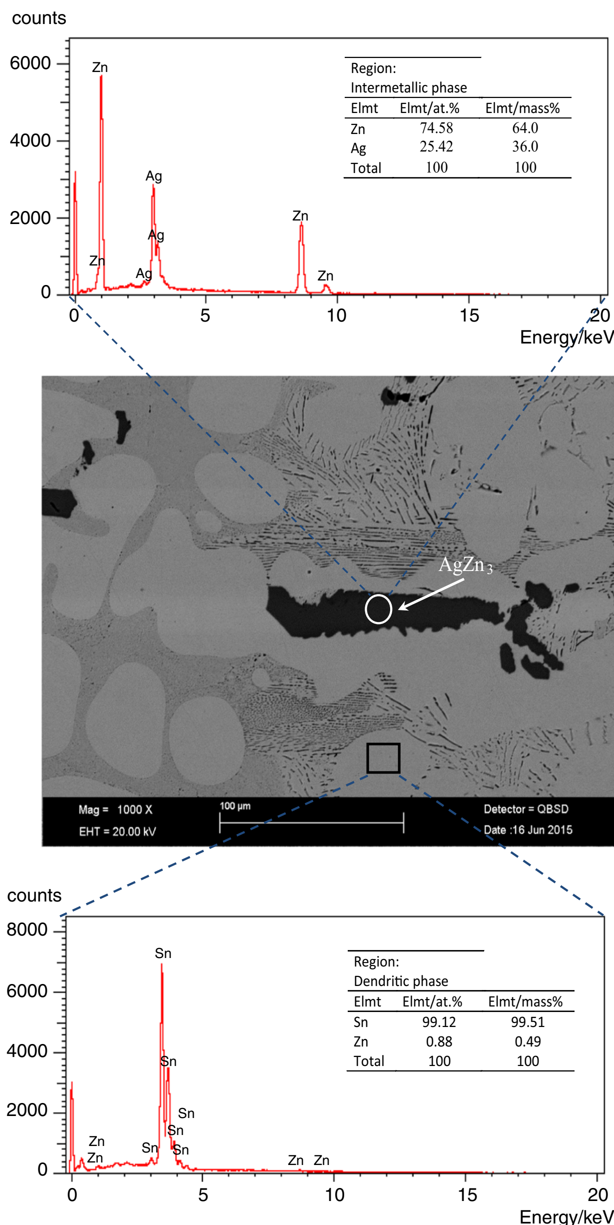

Fig. 2 EDX analysis of the phases containing Ag in the Sn–8.8Zn–3.0Ag alloy

Electrical resistivity

The variation of electrical resistivities of the Sn–Zn–Ag alloys with temperature is given in Fig. 4. As shown in Fig. 4, the resistivities linearly increase with increasing temperature. Also, the dependencies of the electrical resistivities on the Ag content and temperature are given in Fig. 5. As shown in Fig. 5, the resistivity increases with increasing Ag content up to 3.0 mass% and decreases with the addition of 10 mass% Ag. It has been found that Sn–8.8Zn–3.0Ag alloy has the greatest resistivity compared with the other alloys. The relationship between the electrical resistivity and the Ag content is nonlinear. The temperature coefficients of resistivities of the alloys calculated from Eq. (3) and the electrical resistivities measured by different researchers [16, 27–29] in the Sn–Zn–Ag alloys are given in Table 2. As given in Table 2, the electrical resistivity increment with the Ag addition into the Sn–Zn eutectic alloy is found by many researches [16, 28, 29]. Hung et al. [16] found that with the addition of 2.5 mass% Ag into the Sn–9Zn eutectic alloy, the resistivity increased the maximum value compared with the addition of 0.5–2.0 mass% Ag. Gancarz and Pstrus [28] found that an addition of 1.0 mass% Ag into the Sn–8.7Zn eutectic alloy increased the resistivity (12.1 μΩ cm) compared with Sn–8.7Zn (11.7 μΩ cm) and Sn–8.7Zn–0.5Ag (11.9 μΩ cm). Kamal et al. [29] found that with the addition of 1.0 mass% Ag into the Sn–9Zn eutectic alloy, the resistivity increased from 16.2 to 19.9 μΩ cm. Although Ag has the best electrical conductivity compared with Sn and Zn, Ag addition into the Sn–Zn eutectic alloy increases the electrical resistivity up to a certain amount. One of the reasons of this increment is the $AgZn_3$ intermetallic phase formation during solidification. The effect of intermetallics on the electrical resistivity occured in the Sn–Zn–Ag alloys is reported by many researchers [16, 28, 29]. Hung et al. [16] reported that $AgZn_3$ intermetallics and other structural variations resulted in an increment in the electrical resistivity of the Sn–Zn–Ag alloys. Gancarz and Ptsrus [28] reported that small precipitates of $AgZn_3$ increased the electrical resistivity of Sn–Zn–Ag alloys. Also, Kamal et al. [29] reported that the Ag_3Sn and Ag_4Sn intermetallics act as scattering centers for the conduction electrons. As a result of this, the electrical resistivity increases. The intermetallics occured in solid cause impurity effect. As a result, both the grain boundaries and dislocations increase and cause an increase in the electrical resistivities of studied alloys.

Table 1 Composition analysis results of the intermetallic phases

Alloy	Zn/at.%	Ag/at.%	Sn/at.%	Intermetallic phases
Sn–8.8Zn–0.7Ag	80.78	19.22	–	$AgZn_4$
Sn–8.8Zn–1.0Ag	80.61	19.39	–	$AgZn_4$
Sn–8.8Zn–3.0Ag	74.58	25.42	–	$AgZn_3$
Sn–8.8Zn–10.0Ag	59.48	38.23	2.30	–

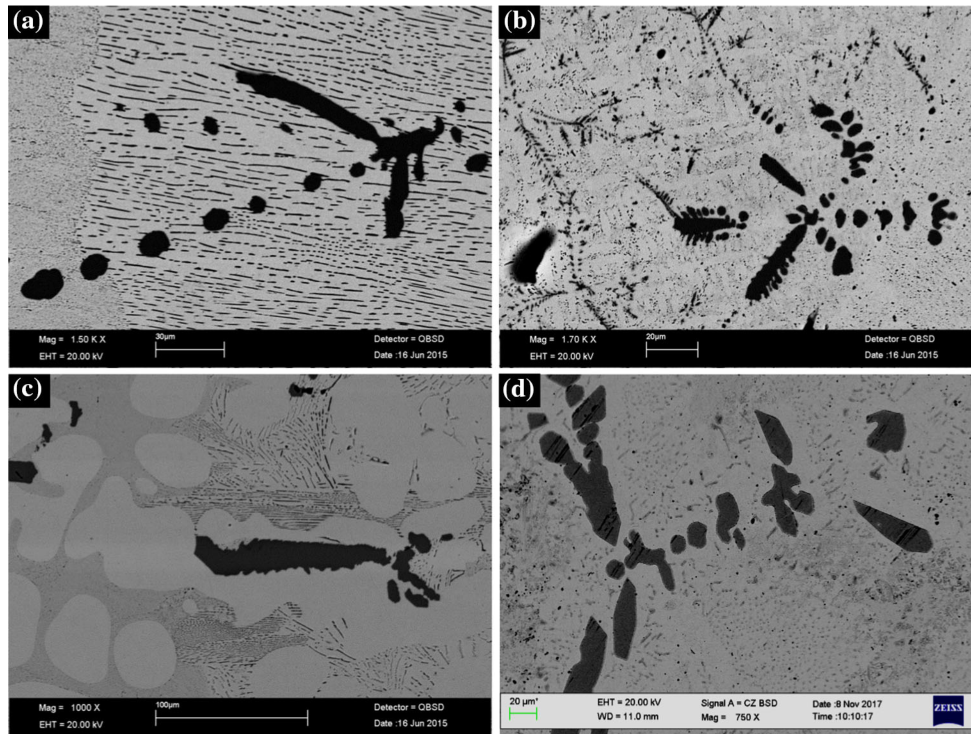

Fig. 3 SEM images of the **a** Sn–8.8Zn–0.7Ag, **b** Sn–8.8Zn–1.0Ag, **c** Sn–8.8Zn–3.0Ag, **d** Sn–8.8Zn–10.0Ag alloys

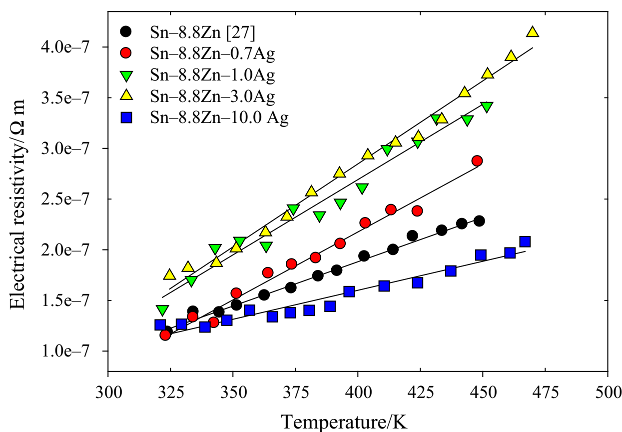

Fig. 4 Variation of electrical resistivities of the Sn–Zn–Ag alloys with temperature

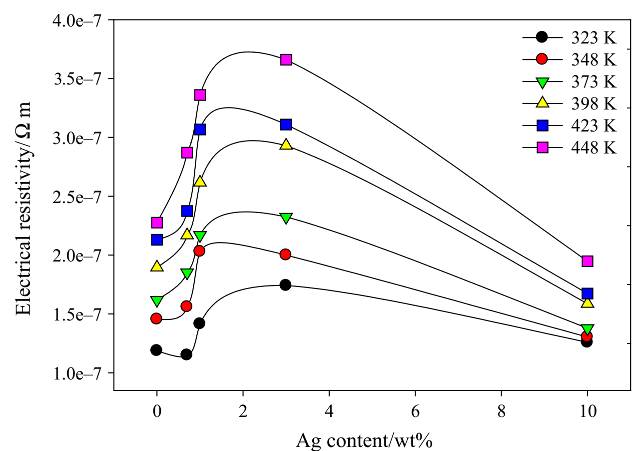

Fig. 5 Dependence of electrical resistivities on the Ag content and temperature

Thermal conductivity

In this work, the thermal conductivity values calculated from Wiedemann–Franz [24] equation is the electronic contribution of the thermal conductivity. The variation of thermal conductivity of the Sn–Zn–Ag alloys with temperature was determined using σ and L values from the

Table 2 Electrical properties of the Sn–Zn–Ag alloys at room temperature

C_0/wt%	α/K^{-1}	ρ/Ω m × 10^{-8}	References
$Sn_{91.2}Zn_{8.8}$	7.34 × 10^{-3}	11.6	[27]
$Sn_{90.5}Zn_{8.8}Ag_{0.7}$	11.96 × 10^{-3}	13.0	This work
$Sn_{90.5}Zn_{9.0}Ag_{0.5}$	–	10.9	[16]
$Sn_{90.8}Zn_{8.7}Ag_{0.5}$	–	11.9	[28]
$Sn_{90.2}Zn_{8.8}Ag_{1.0}$	10.9 × 10^{-3}	13.2	This work
$Sn_{90.0}Zn_{9.0}Ag_{1.0}$	–	10.8	[16]
$Sn_{90.0}Zn_{9.0}Ag_{1.0}$	–	19.9	[29]
$Sn_{90.3}Zn_{8.7}Ag_{1.0}$	–	12.1	[28]
$Sn_{89.5}Zn_{9.0}Ag_{1.5}$	–	11.1	[16]
$Sn_{89.0}Zn_{9.0}Ag_{2.0}$	–	11.0	[16]
$Sn_{88.2}Zn_{8.8}Ag_{3.0}$	9.47 × 10^{-3}	15.0	This work
$Sn_{88.5}Zn_{9.0}Ag_{2.5}$	–	11.3	[16]
$Sn_{81.2}Zn_{8.8}Ag_{10.0}$	4.47 × 10^{-3}	11.9	This work

Wiedemann–Franz equation. The σ values were measured experimentally. The Lorenz value of tin (2.44×10^{-8} W Ω K^{-2} [25]) was used for the determination of thermal conductivity because tin-based alloys were investigated in present work. As shown in Fig. 6, the thermal conductivities decrease with increasing temperature. We may conclude that the temperature increases slower than electrical conductivity decreases. With increase in temperature, both number of carrier electrons and contribution of lattice vibrations increase. Thus, thermal conductivity of a metal is expected to increase. However, because of greater lattice vibrations, electron mobility decreases. The combined effect of these factors leads to very different behavior for different metals and alloys. As mentioned above, in this study thermal

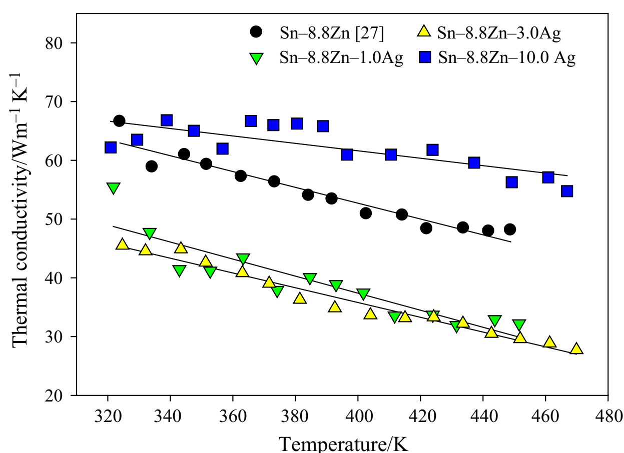

Fig. 6 Variation of thermal conductivities of Sn–Zn–Ag alloys with temperature

conductivities decrease with increasing temperature. Nevertheless, for some intermetallic compounds (Ag_3Sn, Cu_3Sn, Cu_6Sn_5) thermal conductivities increase with increasing temperature. This happens because in the intermetallics, the value of temperature increases quicker than conductivity decreases [30]. The accuracy of the Wiedemann–Franz equation has been examined by several researchers for different metals and alloys [30, 31]. Yao et al. [30] determined that the Wiedemann–Franz equation was found to be well obeyed in intermetallic compounds and solder alloys especially Sn-rich solders. For Sn-based alloys, Yao et al. [30] found that the thermal conductivities decrease with increasing temperature as in this thermal conductivity values calculated from Wiedemann–Franz equation. Aloffson et al. [31] found that a good agreement was found between the calculated thermal conductivity and the experimentally measured thermal conductivity values for the Al–Mg alloys.

Enthalpy and specific heat

Figure 7a–f illustrates the DSC curves of the $Sn_{91.2-x}$–$Zn_{8.8}$–Ag_x ($x = 0.15$–10.0 mass%) solder alloys used in this study. Figure 7a–e indicates that the solidus temperature (T_{onset}) of the $Sn_{91.2-x}$–$Zn_{8.8}$–Ag_x ($x = 0.15$–3.0 mass%) solder alloys is approximately 472.5 K. When 10 mass% Ag is added to the Sn–Zn, the T_{onset} of the $Sn_{81.2}$–$Zn_{8.8}$–Ag_{10} solder alloy increases from 472.5 to 492.5 K, as shown in Fig. 7f. The melting range of the $Sn_{91.2-x}$–$Zn_{8.8}$–Ag_x ($x = 0.15$–3.0 mass%) solder alloys is about 4–5 K, as shown in Fig. 7a–e. The melting range of the $Sn_{81.2}$–$Zn_{8.8}$–Ag_{10} solder alloy is determined approximately 7 K (Fig. 7f). Chang et al. [32] have pointed out that (T_{end}–T_{onset}) of the Sn–37Pb and Sn–9Zn solder alloys is 11.5 and 12.6 K, respectively. $Sn_{91.2-x}$–$Zn_{8.8}$–Ag_x alloys have a narrow melting range which alleviates the occurrence of segregation and hot tear.

The variation of ΔH and ΔC_p calculated from heat flow–temperature curves with Ag content is given in Figs. 8 and 9. As shown in Figs. 8 and 9, the ΔH and the ΔC_p decrease with an increasing content of Ag. When the Ag content is increased from 0.15 to 10.0 mass%, the ΔH and the ΔC_p decreased from 70.81 to 58.20 J g^{-1} and 0.355 to 0.265 J g^{-1} K^{-1}, respectively. The comparisons of ΔH and ΔC_p obtained by the present work with the ΔH and the ΔC_p values predicted by Ref. [33] are given in Figs. 10, 11 and Table 3. Wu et al. [33] measured the ΔC_p and the ΔH using differential scanning calorimetry at 303 K. Nevertheless, in the present work ΔC_p and ΔH were determined for the melting temperatures of the alloys. For comparison, the ΔC_p and ΔH values measured from Wu et al. [33] are predicted for the melting temperatures. The exponent value (0.05) of C_0 obtained by the linear regression analysis from

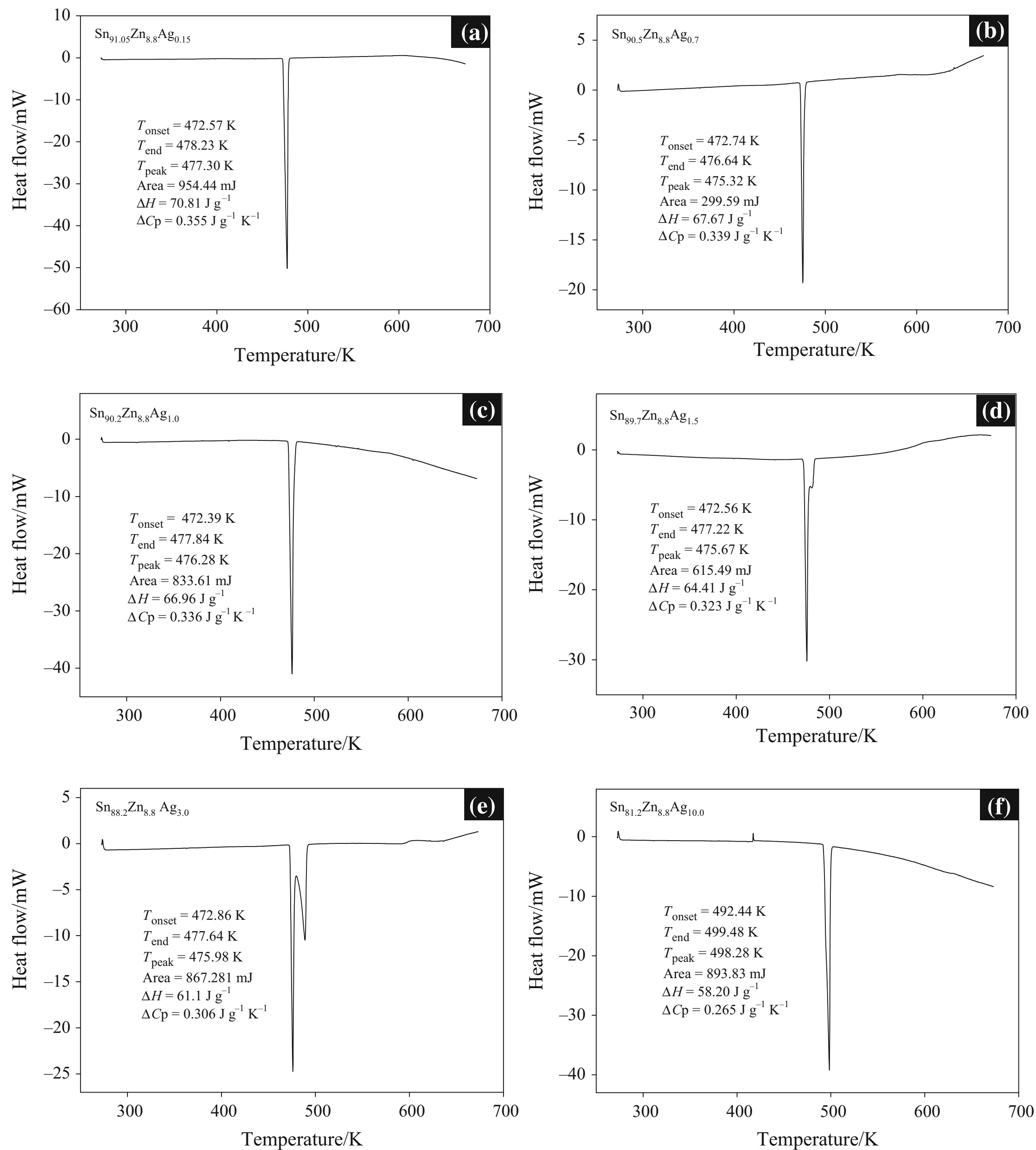

Fig. 7 Heat flow–temperature curve of the alloys; **a** $Sn_{91.05}Zn_{8.8}Ag_{0.15}$, **b** $Sn_{90.5}Zn_{8.8}Ag_{0.7}$, **c** $Sn_{90.2}Zn_{8.8}Ag_{1.0}$, **d** $Sn_{89.7}Zn_{8.8}Ag_{1.5}$, **e** $Sn_{88.2}Zn_{8.8}Ag_{3.0}$, **f** $Sn_{81.2}Zn_{8.8}Ag_{10.0}$

this work as a function of ΔC_p and ΔH is in good agreement with the predicted values of 0.04 obtained by Wu et al. [33].

As mentioned in "Measurement of enthalpy and specific heat" section, the DSC thermal analysis was performed with a heating rate of 10 K min^{-1}. A heat treatment parameter heating rate has effect on thermal properties of the materials such as melting temperature, enthalpy and specific heat. Xiao et al. [34] reported that the onset temperature and peak temperature increase with increasing heating rate. Also the enthalpy changes with heating rate [34]. Srivastava et al. [35] found that an increment in the heating rate causes an increment of the glass transition temperature, crystallization temperature and peak crystallization temperature.

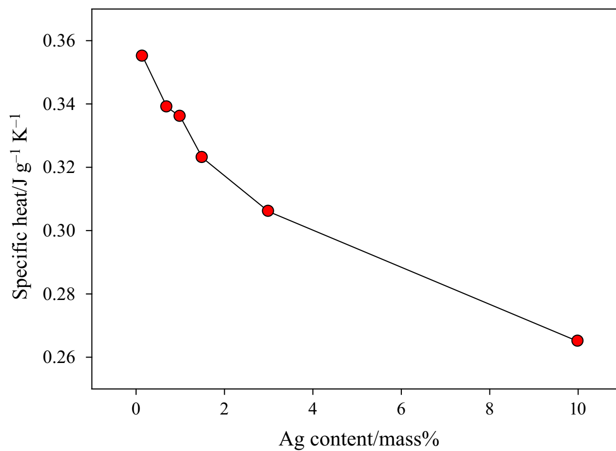

Fig. 8 Variation of specific heat with Ag content

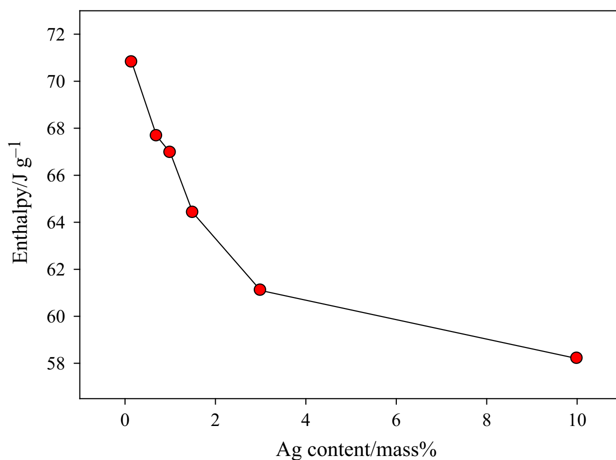

Fig. 9 Variation of enthalpy with Ag content

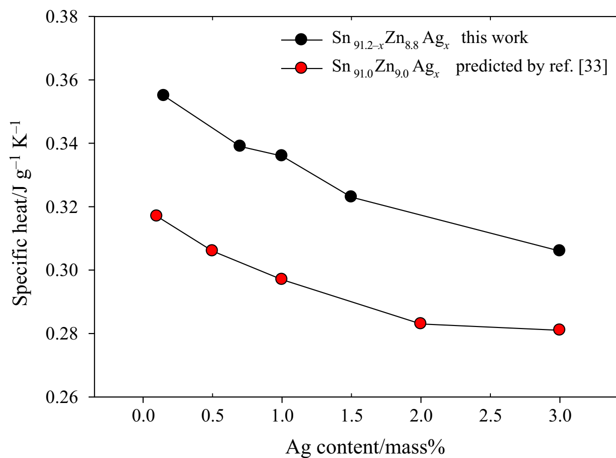

Fig. 10 Comparison of ΔC_p obtained by the present work with the ΔC_p values predicted by Ref. [33] for melting temperature

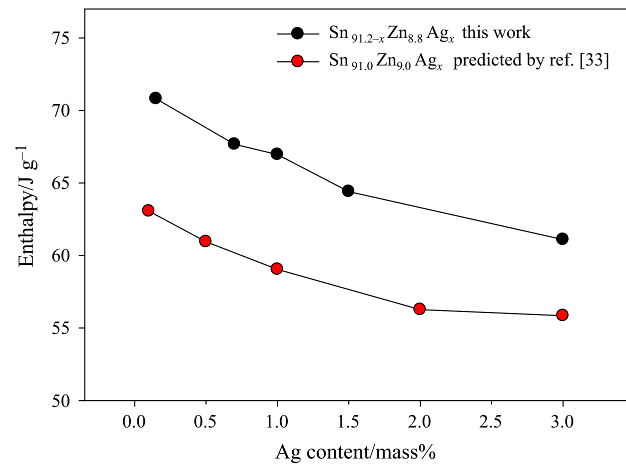

Fig. 11 Comparison of ΔH obtained by the present work with the ΔH values predicted by Ref. [33] for melting temperature

Table 3 ΔH and the ΔC_p values of the Sn–Zn–Ag alloys

C_0/wt%	ΔH/J g^{-1}	ΔC_p/J g^{-1} K^{-1}	References
$Sn_{91.2}Zn_{8.8}$	73.11	0.366	[27]
$Sn_{91.05}Zn_{8.8}Ag_{0.15}$	70.81	0.355	This work
$Sn_{91.0}Zn_{9.0}Ag_{0.1}$	63.06	0.317	[33]
$Sn_{90.5}Zn_{8.8}Ag_{0.7}$	67.67	0.339	This work
$Sn_{91.0}Zn_{9.0}Ag_{0.5}$	60.95	0.306	[33]
$Sn_{90.2}Zn_{8.8}Ag_{1.0}$	66.96	0.336	This work
$Sn_{91.0}Zn_{9.0}Ag_{1.0}$	59.04	0.297	[33]
$Sn_{89.7}Zn_{8.8}Ag_{1.5}$	64.41	0.323	This work
$Sn_{91.0}Zn_{9.0}Ag_{2.0}$	56.27	0.283	[33]
$Sn_{88.2}Zn_{8.8}Ag_{3.0}$	61.10	0.306	This work
$Sn_{91.0}Zn_{9.0}Ag_{3.0}$	55.85	0.281	[33]
$Sn_{81.2}Zn_{8.8}Ag_{10.0}$	58.20	0.265	This work

Conclusions

Sn–Zn–Ag alloys were directionally solidified upwards at a constant solidification conditions ($G = 4.16$ K mm^{-1}, $V = 41.5$ µm s^{-1}) in a Bridgman-type directional solidification furnace. The results are summarized as follows:

1. The resistivities of the alloys linearly increased with increasing temperature. The resistivity increased up to 3.0 mass% Ag addition and decreased with the addition 10.0 mass% Ag. Sn–8.8Zn–3.0Ag alloy has the greatest resistivity compared with the other alloys. The $AgZn_3$ intermetallics occured in the Sn–8.8Zn–3.0Ag alloy caused an increase in the electrical resistivity.
2. The variation of thermal conductivities of the studied alloys with temperature was determined by using the

Wiedemann–Franz equation. The thermal conductivities decreased with increasing temperature.

3. The solidus temperatures of the $Sn_{91.2-x}$–$Zn_{8.8}$–Ag_x alloys ($x = 0.15$–3.0 mass%) and $Sn_{81.2}$–$Zn_{8.8}$–Ag_{10} solder alloy are 472.5 and 492.5 K, respectively. The liquidus temperatures of the $Sn_{91.2-x}$–$Zn_{8.8}$–Ag_x alloys ($x = 0.15$–3.0 mass%) and $Sn_{81.2}$–$Zn_{8.8}$–Ag_{10} solder alloy are 477.5 and 499.5 K, respectively.
4. The enthalpy and the specific heat decreased with increasing content of Ag. When the Ag content was increased from 0.15 to 10.0 mass%, the ΔH and the ΔC_p decreased from 70.81 to 58.20 J g^{-1} and 0.355 to 0.265 J g^{-1} K^{-1}, respectively.

Acknowledgements This project was supported by the Niğde Ömer Halisdemir University Scientific Research Project Unit under Contract No: FEB 2013/18. The authors would like to thank to Niğde University Scientific Research Project Unit for their financial support.

References

1. Verhoeven JD. Fundamentals of physical metallurgy. New York: Wiley; 1975.
2. Kurz W, Fisher DJ. Fundamentals of solidification. 3rd ed. Aedermannsdorf: Trans Tech Publications; 1989.
3. Gündüz M, Çadırlı E. Directional solidification of aluminium-copper alloys. Mater Sci Eng A. 2002;327:167–85.
4. Peng P, Li X, Su Y, Li J, Guo J, Fu H. Dependence of micro-hardness on solidification processing parameters and dendritic spacing in directionally solidified Sn–Ni peritectic alloys. J Alloy Compd. 2015;618:49–55.
5. Dong S, Chen R, Guo J, Ding H, Su Y, Fu H. Microstructure control and mechanical properties of Ti44Al6Nb1.0Cr2.0V alloy by cold crucible directional solidification. Mater Sci Eng A. 2014;614:67–74.
6. Hu X, Li K, Min Z. Microstructure evolution and mechanical properties of Sn0.7Cu0.7Bi lead-free solders produced by directional solidification. J Alloy Compd. 2013;566:239–45.
7. Yan Y, Ding H, Kang Y, Song J. Microstructure evolution and mechanical properties of Nb–Si based alloy processed by electromagnetic cold crucible directional solidification. Mater Des. 2014;55:450–5.
8. Shnawah DA, Said SBM, Sabri MFM, Badruddin IA, Che FX. High-reliability low-Ag content Sn–Ag–Cu solder joints for electronics applications. J Electron Mater. 2012;41:2631–58.
9. Che FX, Pang JHL. Characterization of IMC layer and its effect on thermomechanical fatigue life of Sn–3.8Ag–0.7Cu solder joints. J Alloys Compd. 2012;541:6–13.
10. Alam ME, Nai SML, Gupta M. Development of high strength Sn–Cu solder using copper particles at nanolength scale. J Alloys Compd. 2009;476:199–206.
11. Bui QV, Jung SB. Characterization of low speed shear test reliability of Sn–1.0Ag XCe/ENEPIG solder joint. J Alloys Compd. 2013;560:54–61.
12. Lee JE, Kim KS, Inoue M, Jiang J, Suganuma K. Effects of Ag and Cu addition on microstructural properties and oxidation resistance of Sn–Zn eutectic alloy. J Alloy Compd. 2008;454:310–20.
13. Wenxue C, Songbai X, Hui W, Yuhua H. Effects of Ag on properties of Sn–9Zn lead-free solder. Rare Metal Mat Eng. 2010;39:1702–6.
14. Tsai YL, Hwang WS. Solidification behavior of Sn–9Zn–xAg lead-free solder alloys. Mater Sci Eng A. 2005;413–414:312–6.
15. Song JM, Lui TS, Lan GF, Chen LH. Resonant vibration behavior of Sn–Zn–Ag solder alloys. J Alloy Compd. 2004;379:233–9.
16. Hung FY, Wang CJ, Huang SM, Chen LH, Lui TS. Thermo-electrical characteristics and tensile properties of Sn–9Zn–xAg lead-free solders. J Alloy Compd. 2006;420:193–8.
17. El-Daly AA, Hammad AE. Effects of small addition of Ag and/or Cu on the microstructure and properties of Sn–9Zn lead-free solders. Mater Sci Eng A. 2010;527:5212–9.
18. Ahmed M, Fouzder T, Sharif A, Gain AK, Chan YC. Influence of Ag micro-particle additions on the microstructure, hardness and tensile properties of Sn–9Zn binary eutectic solder alloy. Microelectron Reliab. 2010;50:1134–41.
19. El-Daly AA, Hammad AE. Elastic properties and thermal behavior of Sn–Zn based lead-free solder alloys. J Alloy Compd. 2010;505:793–800.
20. Şahin M. The directional solidification of binary and ternary metallic alloys and investigation the physical properties of them. Ph.D. thesis, Niğde University, Nigde, 2012.
21. Smiths FM. Measurement of sheet resistivities with the four-point probe. Bell Syst Technol J. 1958;37:711–8.
22. Topsoe H. Geometric factor in four-point resistivity measurement. Semiconductor division no. 472-13 (Vedbaek), 1968:38.
23. Çolak H, Türkoğlu O. Structural and electrical studies of Cu-doped CdO prepared by solid state reaction. Mater Sci Semicond Process. 2013;16:712–7.
24. Kittel C. Introduction to solid state physics. 6th ed. New York: Wiley; 1965.
25. Kumar GS, Prasad G, Pohl RO. Review experimental determinations of the Lorenz number. J Mater Sci. 1993;28:4261–72.
26. Ohtani H, Miyashita M, Ishida K. Thermodynamic study of phase equilibria in the Sn–Ag–Zn system. J Jpn Instrum Methods. 1999;63:685–94.
27. Karakurt F. The directional solidification of Ag added Sn–8.8 wt% Zn eutectic alloy and investigation the physical properties. M.Sc. thesis, Niğde University, Nigde, 2015.
28. Gancarz T, Pstrus J. Characteristics of Sn–Zn cast alloys with the addition of Ag and Cu. Arch Metall Mater. 2015;60:1603–7.
29. Kamal M, Meikhail MS, El-Bediwi AB, Gouda ES. Study of structural changes and properties for Sn–Zn_9 lead-free solder alloy with addition of different alloying elements. Radiat Eff Defect Solids. 2005;160:45–52.
30. Yao Y, Fry J, Fine ME, Keer LM. The Wiedemann–Franz–Lorenz relation for lead-free solder and intermetallic materials. Acta Mater. 2013;61:1525–36.
31. Olafsson P, Sandstrom R, Karlsson A. Comparison of experimental, calculated and observed values for electrical and thermal conductivity of aluminium alloys. J Mat Sci. 1997;32:4383–90.
32. Chang TC, Hon MH, Wang MC. Thermal characteristics and intermetallic compounds formed at Sn–9Zn–0.5Ag/Cu interface. Mater Trans. 2004;45:606–13.
33. Wu YK, Lin KL, Salam B. Specific heat capacities of Sn–Zn-based solders and Sn–Ag–Cu solders measured using differential scanning calorimetry. J Electron Mater. 2009;38:227–30.
34. Xiao LB, Zhao FQ, Luo Y, Li N, Gao HX, Xue YQ, Cui ZX, Hu RZ. Thermal behavior and safety of dihydroxylammonium 5,5′-bistetrazole-1,1′-diolate. J Therm Anal Calorim. 2016;123:653–7.
35. Srivastava A, Tiwari SN, Upadhyay AN, Zulfequar M, Khan SA. First-order phase transformation and structural studies in $Se_{85-}In_{15-x}Zn_x$ chalcogenide glasses. Therm Anal Calorim. 2017;129:1435–44.